Engineering Science and Technology, an International Journal 47 (2023) 101556

Contents lists available at ScienceDirect

Engineering Science and Technology, an International Journal

journal homepage: www.elsevier.com/locate/jestch

# The effect of number of nanoparticles on atomic behavior and aggregation of CuO/water nanofluid flow in microchannels using molecular dynamics simulation

Langzhun Ze [a,*], F. Al-dolaimy [b], S. Mohammad Sajadi [c], Maytham T. Qasim [d], Ahmed Hussien Alawadi [e,f,g], Reza Balali Dehkordi [h], Ali Alsalamy [i], Roozbeh Sabetvand [j], Maboud Hekmatifar [h]

[a] Experimental Teaching Department, Northwest Minzu University, Lanzhou, Gansu 730030, China
[b] Al-Zahraa University for Women, Karbala, Iraq
[c] Department of Nutrition, Cihan University-Erbil, Kurdistan Region, Iraq
[d] Department of Anesthesia, College of Health and Medical Technololgy, Al-Ayen University, Thi-Qar, Iraq
[e] College of Technical Engineering, The Islamic University, Najaf, Iraq
[f] College of Technical Engineering, The Islamic University of Al Diwaniyah, Iraq
[g] College of Technical Engineering, The Islamic University of Babylon, Iraq
[h] Department of Mechanical Engineering, Khomeinishahr Branch, Islamic Azad University, Khomeinishahr, Iran
[i] College of Technical Engineering, Imam Ja'afar Al-Sadiq University, Al-Muthanna 66002, Iraq
[j] Department of Energy Engineering and Physics, Faculty of Condensed Matter Physics, Amirkabir University of Technology, Tehran, Iran

ARTICLE INFO

*Keywords:*
Nanofluid
Microchannel
$H_2O$/CuO nanofluid
Molecular dynamics
Aggregation

ABSTRACT

A nanofluid (NF) is a mixture of metallic or non-metallic nanoparticles (NPs) suspended in a fluid. The high activity and energy of the surface atoms of NPs cause them to stick together and aggregate in the base fluid (BF). This leads to instability, changes in the NF concentration, and fouling and obstruction of the flow path, which reduces the NF's thermal conductivity (TC). In this study, the effect of copper oxide NPs on atomic behavior and the aggregation procedure in a water/CuO NF flow in a microchannel was explained using a Molecular Dynamics (MD) simulation procedure. For this purpose, various physical parameters, such as density, temperature, velocity, aggregation time (AT), and potential energy (PE), were calculated. The results show that after 1 ns, the temperature and PE converged to 300 K and −553088 eV. By CuO NPs number increasing among $H_2O$ molecules, the maximum ratio of density, temperature, and V profiles reached 1.60 g/cm$^3$, 0.0122 Å/ps, and 303 values. The aggregation process in simulated NF was varied by these atomic changes. From a numerical point of view, by CuO NPs number increasing from 2 to 3 NPs, the AT reduced by 1.15 ns to 1.01 ns. Furthermore, this atomic evolution was investigated by PE changed from −652411 to −660258 eV.

## 1. Introduction

A mixture of metallic or non-metallic NPs suspended in a BF is called NF. According to the researcher's experimental results, adding NPs, such as CuO, $Fe_3O_4$, MgO, etc., improved the properties of the BF [1–5]. Fabricating stable, uniform, durable, and long-lasting NFs in small and miniature equipment, such as microchannels, micro coolers, and micro-radiators are key points to prepare NFs [6,7]. Among the NPs used in NFs, research showed that CuO/water (0.698 W/m.K) NF [8], in terms of their high TC compared to $Fe_3O_4$/water (0.7 W/m.K) [9], and MgO/water (0.598 W/m.K) NF [10], improve the thermal behavior of base layer. It had the advantage of using more eco-friendly materials, being cheaper than chemical synthesis, simpler, more rapid and sustainable [11].

MD simulation is a critical tool for studying the structure and

*Abbreviations:* NPs, Nanoparticles; NFs, Nanofluid; BF, Base fluid; TC, Thermal conductivity; AT, Aggregation time; PE, Potential energy; D, Molecular Dynamics; CuO, Copper Oxide; UFF, Universal Force Field; EAM, Embedded-Atom Method; LJ, Lennard-Jones; LAMMPS, Large scale atomic/molecular massively parallel simulation; ns, Nanosecond; eV, Electron Volt.

* Corresponding author.
*E-mail address:* by127706@163.com (L. Ze).

https://doi.org/10.1016/j.jestch.2023.101556
Received 13 November 2022; Received in revised form 12 September 2023; Accepted 18 October 2023
Available online 27 October 2023

**Nomenclature**

| | |
|---|---|
| $r_{ij}$ | The distance between particles (m) |
| $u_i$ | The potential of a particle (eV) |
| $\varepsilon_{ij}$ | Depth of the potential well (Kcal/mol) |
| $\sigma_{ij}$ | Finite distance in which the potential is zero(Å) |
| r | The distance of the particles from each other |
| $U_{ij}$ | The electric potential (eV) |
| V | The total volume of particles ($Å^3$) |
| $k_B$ | Boltzmann constant ($1.380649 \times 10^{-23}$ $J{\cdot}K^{-1}$) |
| T | The system temperature (K) |
| $m_i$ | The mass of the particle (g) |
| $a_i$ | The acceleration of the particle ($m{\cdot}s^{-2}$) |
| $N_{fs}$ | The number of degrees of freedom |
| $F_\alpha$ | Constant coefficient between 0 and 1 |
| $\rho_\beta$ | An attraction force caused by the presence of particles in the simulated box |
| $\phi_\beta$ | A repulsive force caused by atomic charge density |
| $k_r$ | Oscillator constant |
| $r_0$ | Oscillator's bond length |
| $k_\theta$ | Angular oscillator's constant |
| $\theta_0$ | Equilibrium value of the oscillator's angle |
| t | MD simulation time |

**Table 1**
The $\sigma_{ij}$ and $\varepsilon_{ij}$ constants for Lennard-Jones potential in various atoms simulation using MD approach [54,55].

| Atom | $\sigma_{ij}$ (Å) | $\varepsilon_{ij}$ (kcal/mol) |
|---|---|---|
| O | 3.166 | 0.1553 |
| H | 0.000 | 0.000 |
| Cu | 3.495 | 0.005 |
| Pt | 2.754 | 0.008 |

**Table 2**
The all simulation parameters of this study.

| Parameter | Value |
|---|---|
| Initial Temperature | 300 K |
| Initial Pressure | 1 bar |
| External force | 0.02 eV/Å |
| Number of atoms | 1,889,321 atoms |
| Size of CuO | 50 nm |
| Simulation box size | $0.75 \times 0.3 \times 0.3$ $\mu m^3$ |
| Simulation time | 5 ns |

function of biological macromolecules. It is a computational simulation framework in which particles and atoms interact with each other under known laws of physics for a specific time, allowing for the observation of the motion of atoms [12–14]. Studies showed that various factors, including height, temperature, microchannel wall layers, type, size, number of NPs, and electric field, can affect fluid flow [7,15–17].

In their study, Ahadian et al. [18] utilized the MD simulation approach to investigate the flow through a microchannel. The results indicate that the wall material and its interaction with BF had a significant effect on fluid flow in the microchannel. Platinum is a widely used chemical element with the symbol Pt. It is an expensive, dense, flexible metal that is largely inert. It can dissipate heat well which is resistant to the effects of weather, allowing it to withstand high temperatures for extended periods [19]. Platinum is one of the least reactive metals and has significant corrosion resistance, even at high temperatures. For this reason, it is considered a noble metal which is typically found in pure form in nature. Noble metals are a group of metals that exhibit resistance to corrosion and oxidation in humid air [20]. NF was promising in various practical applications, and their behavior depends on the dispersion of NPs in the NF arrangement [21–24]. Due to the high activity and energy of the surface atoms of NPs, they tend to stick together and aggregate in BF, resulting in instability, changes in the NF concentration, fouling and obstruction of the flow path, and a reduction in the NF's TC [25,26]. The demand for enhanced coolants with higher performance is driven by increasing global competition, faster operating speeds, and device miniaturization [27]. The TC of NFs attracted attention in the past decade due to their use in heat transfer. Numerous studies demonstrated a significant improvement in TC in NFs. However, some recent studies showed that the increase in TC was consistent with the expectations of the effective medium theory [28]. Several possible mechanisms were proposed to explain the extensive data spectrum. Research suggests that an increase in aggregation can result in a significant increase in TC. However, in some cases, an increase in aggregation can lead to a decrease in TC. Shima et al. [29] investigated the effect of aggregation on the TC of CuO and $Fe_3O_4$ NFs. The results show that in the absence of stabilizers, the aggregation and subsequent settling of CuO NF led to a decrease in TC over time. This is due to the fact that aggregation caused channel clogging and an increase in thermal resistance. Therefore, it was essential to investigate the aggregation and TC in micro dimensions and microchannels. Various parameters, such as NPs ratio and sizes, could be changed to properly dispersion NPs in BFs. So, optimized NPs ratio performance was important for appropriate dispersion and NF stability [30–32]. Kang et al. [33] utilized MD modeling to study the effect of NP aggregation on the thermal properties of NFs. Additional NPs were added to the simulation box to enable modeling of NP aggregation. The results show that various NP cluster arrangements resulted in different increases in TC and viscosity in the NF. Investigating the effect of $Fe_3O_4$ NPs on NF aggregation was done by Dehkordi et al. [34]. The results show that the maximum rates of density, velocity, and temperature profiles increased to 1.675 $g/cm^3$, 0.012 Å/ps, and 712 K rates, respectively, by increasing the NP number from 1 to 3. Similarly, Shen et al. [35] investigated the effect of ferrite NPs on the atomic behavior of $H_2O$ in a channel with platinum walls. The findings suggest that as the number of NPs increased, the interaction between the fluid particles and the walls led to the aggregation of fluid particles in the vicinity of channel walls.

The addition of NPs to the BF was shown to improve its thermal and atomic behavior, as observed from the review of articles. Additionally, various factors, including NP size, type, and quantity, have an effect on these properties. Increasing the size and number of NPs increased the likelihood of aggregation.

In this study, MD was utilized to examine how the quantity of NPs affected the atomic behavior and aggregation of NF consisting of CuO and water. For this purpose, three NPs were used, and investigations were conducted into how the number of NPs affected density, velocity, temperature, potential energy, and clumping time.

## 2. Simulation details

MD simulation is a powerful tool for studying fluid flow in microchannels. The main principle of this method is to solve Newton's equations by considering the potential for interaction between molecules and external factors. Compared to other nanoscale degradation methods, MD simulations are effective and accurate methods for studying flow behaviors in micro and nanochannels. The atomic behavior of $H_2O$/CuO NF in Pt microchannel in an external electric field was examined using the MD simulation. The simulation box size was considered to be $0.75 \times 0.3 \times 0.3$ $\mu m^3$. Increasing the size of the simulation box while maintaining density results in an increase in the number of particles in the system and, consequently, the number of interactions to be calculated. Therefore, the size of the simulation box should not be too big or too small. In this study, the size of the simulation box was chosen based on previous references and to minimize the

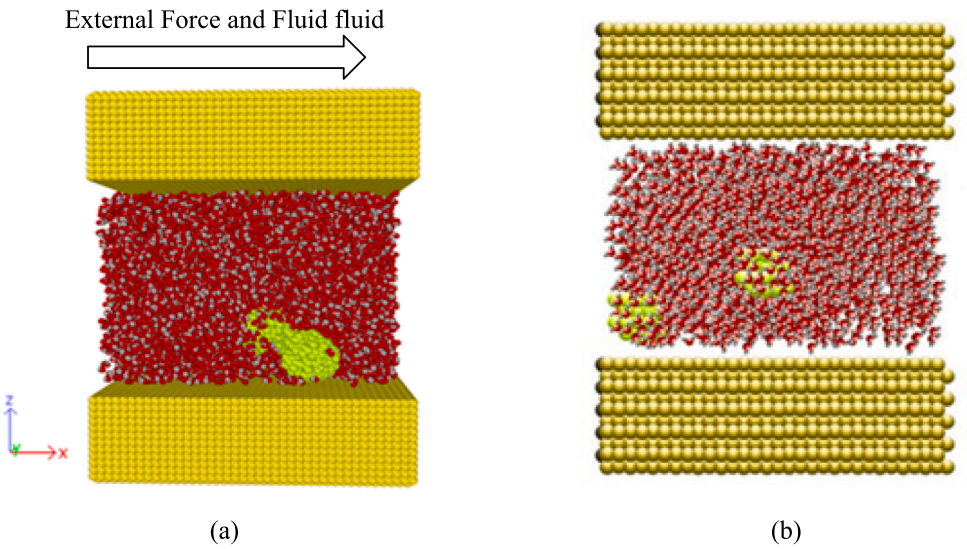


**Fig. 1.** Atomic representation of $H_2O$/CuO NF and Pt microchannel a) befor and b) after 1 ns.

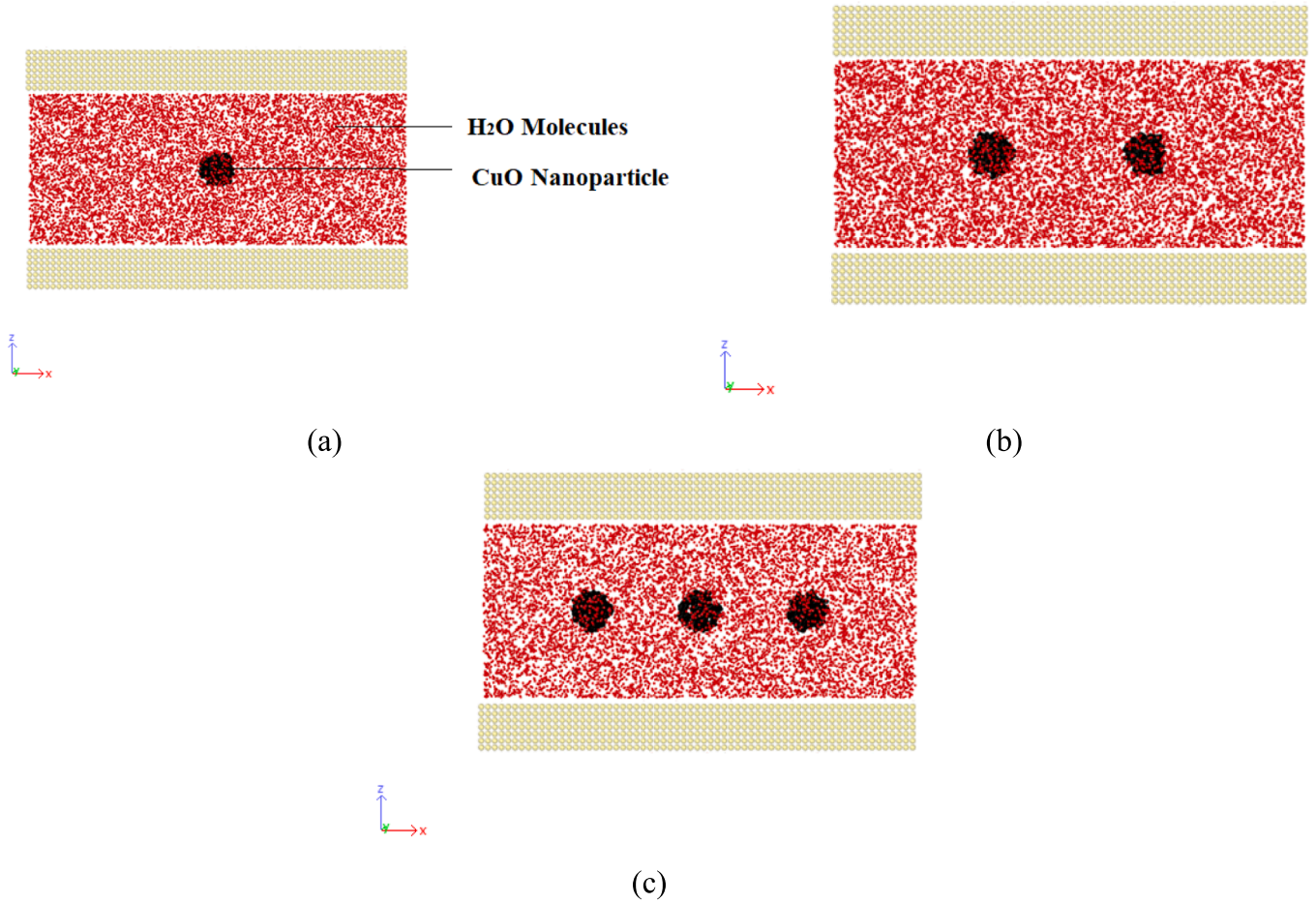


**Fig. 2.** Atomic representation of $H_2O$/CuO NF and Pt microchannel in the presence of various numbers of NPs.

number of simulation runs [34,36].

Then, the water flow was modeled by the simple point charge (SPC) model, and the flow results were evaluated. Based on the researchers' results to study the properties of water molecules using MD, the SPC model's simulation results were close to real and experimental data [37–39]. Furthermore, sites performed for positive charges and electrostatic interactions on hydrogen were equivalent to a properly negative charge added to an oxygen atom [40]. Hence, the structure was stable. SCP model provided a way to advance our understanding of the microscopic mechanism which determined heat transfer in water. Consequently, SPC method was used in this research.

In the Z-orientation, the boundary conditions is fixed and in the X

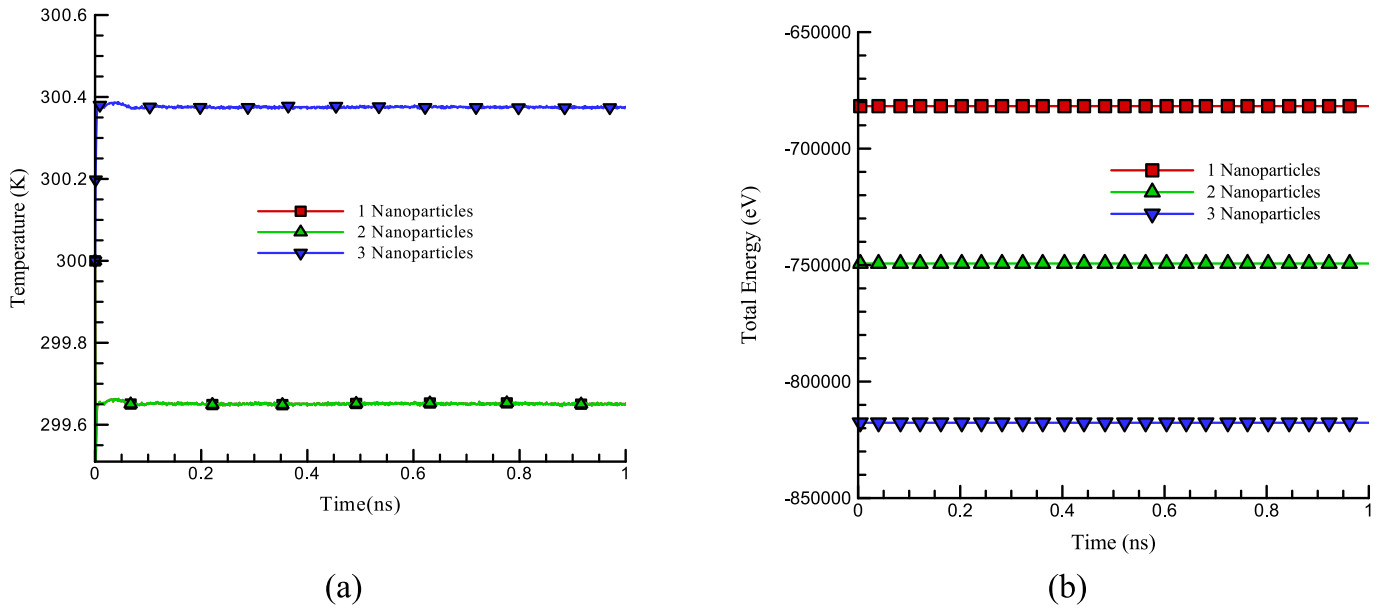


**Fig. 3.** a) Temperature and b) Total energy alteration of $H_2O$/CuO NF at Pt microchannel at different CuO NPs.

**Table 3**
The PE value of $H_2O$/CuO NF and Pt microchannel system in the presence of various CuO NPs after t = 1 ns.

| Number of NPs | Temperature (k) | PE(eV) |
|---|---|---|
| 1 | 299.65 | −533791 |
| 2 | 299.66 | −542811 |
| 3 | 300.37 | −553088 |

and Y orientations were considered to be periodic. The X direction moved in the same direction as the fluid flow. As a result, for every particle that exited the system, an identical particle entered from the other side. Therefore, the total number of atoms remained constant until the end of the simulation and the initial temperature was set to $T_0 = 300$ K. Finally, adding CuO NPs to the fluid structure, system evolution, and flow in the microchannel were evaluated. (Copper oxide NPs were simulated with a spherical structure with a radius of 50 nm). The size of the NPs was selected based on the relevant literature [41,42]. Copper oxide NPs can range in size from 50 nm to 80 nm. Choosing a larger NP size may increase aggregation and clogging of the microchannel [43]. In this study, NPs with a size of 50 nm were selected.

The simulated structure contained 1,889,321 atoms. After determining the number and initial positions of BF, the initial location, and velocity of the particles were established. An external force with magnitude of 0.02 eV/Å applied in X direction to the nanofluid to flow inside the channel. The intermolecular forces were then calculated based on the potential function, and the simulation conditions were applied. The equations of motion were subsequently integrated, and the new momentum and velocity of the particles were recorded at each moment. This loop was continuously repeated until the system reached equilibrium, and finally, the average values of thermodynamic quantities and the simulation outputs were checked. MD simulations procedure was fulfilled using this law and Velocity-Verlet proposition to coordinate Newton's law [44–46].

Discover program offers a number of ways to regulate pressure, and temperature. Different statistical ensembles may be produced depending on which state variables (such as the energy (E), volume (V), temperature (T), pressure (P), and particle number (N)) were maintained constant. The averages or changes of these values across the ensemble created may then be used to compute a range of structural, energy, and dynamic properties [47].

The available ensembles are:
Constant energy, constant volume (NVE).
Constant temperature, constant volume (NVT) (default).
Constant temperature, constant pressure (NPT).
In all ensembles, the number of particles is conserved.

The constant-temperature, constant-volume ensemble (NVT), also known as the canonical ensemble, was the default ensemble used by the Discover program. During the initialization step, direct temperature scaling was used to regulate the temperature, and temperature-bath coupling was used during the data collection stage to create the ensemble [48]. The volume was maintained throughout the entire simulation run. When molecules were searched for their conformation in a vacuum without periodic boundary requirements, the constant-temperature constant-volume ensemble was the best option. Without periodic boundary conditions, it was not possible to define volume, pressure, and density. Constant pressure dynamics cannot be performed in this case. The constant-temperature constant-volume ensemble had the advantage of minimal trajectory disruption because it did not require a connection to a pressure bath, even when periodic boundary conditions were employed [49].

The simulation system was kept in volume and temperature. A Canonical (NVT) ensemble was used for this purpose. Nose-Hoover thermostat had bridged temperature [50–52]. The system's energy was minimized and simulated for 1 ns (equilibration time) in thermodynamic mode. This thermostat was executed for getting to the equilibrium phase for t = 1 ns. Still, MD simulations were accomplished till t = 4 ns afterward using a micro-canonical (NVE) ensemble to the time evolution detection CuO NPs aggregation process in the MD box. Therefore, the total duration of the simulation was equal to 5 ns, which was enough to study and observe various atomic phenomena, such as atomic behavior and aggregation in simulated NPs.s

Applying intermolecular potentials was one of the basic issues to solve MD. The present study used Universal Force Field (UFF) for fluid, NP, and wall molecules. Moreover, the potential of Embedded-Atom Method (EAM) was used to estimate the internal interplay of metal particles [37,53–55]. UFF force field was represented by Lennard-Jones potential. Lennard-Jones equation used for non-bond interaction among different atoms was shown as follows [56]:

$$U_{LJ} = 4\varepsilon_{ij}\left[\left(\frac{\sigma_{ij}}{r}\right)^{12} - \left(\frac{\sigma_{ij}}{r}\right)^{6}\right] \quad (1)$$

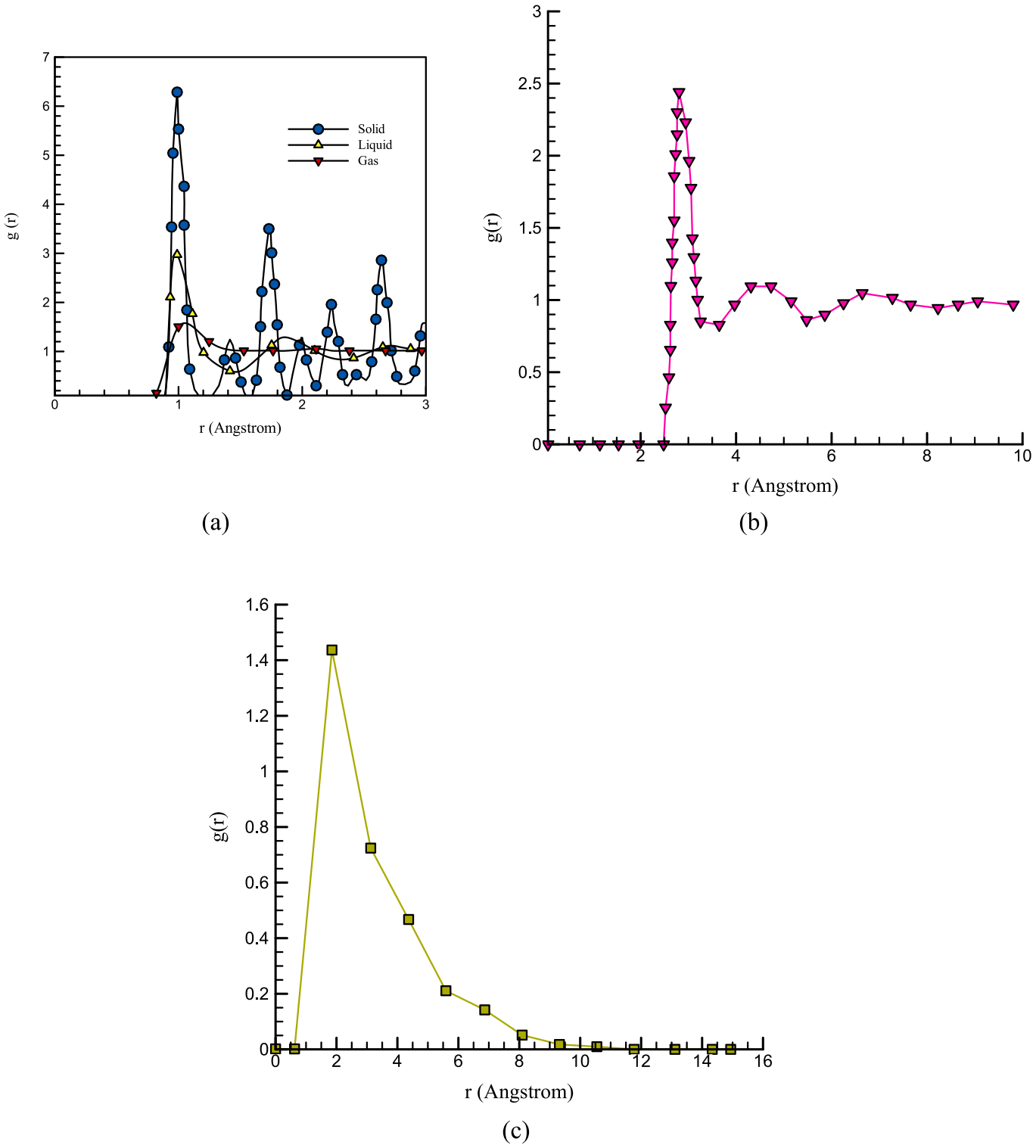


**Fig. 4.** A) the changes in the rdf with the change in the phase of the simulated samples [65]:, b) The radial distribution function of O atom in $H_2O$, and c) The radial distribution function of Cu-O.

The $\sigma_{ij}$ and $\varepsilon_{ij}$ constants for different atoms are detailed in Table 1 [54,55].

A basic oscillator with taking after formalism was performed to define these types of interactions [57],

$$E_r = \frac{1}{2}k_r(r - r_0)^2 \quad (2)$$

In Eq. (2), $k_r$ is a simple constant of an oscillator, and $r_0$ defines the oscillator's band length in the equilibrium state. Moreover, a simple angular oscillator was applied to the definition of bond-angle interaction in structures based on Eq.3 [58],

$$E_\theta = \frac{1}{2}k_\theta(\theta - \theta_0)^2 \quad (3)$$

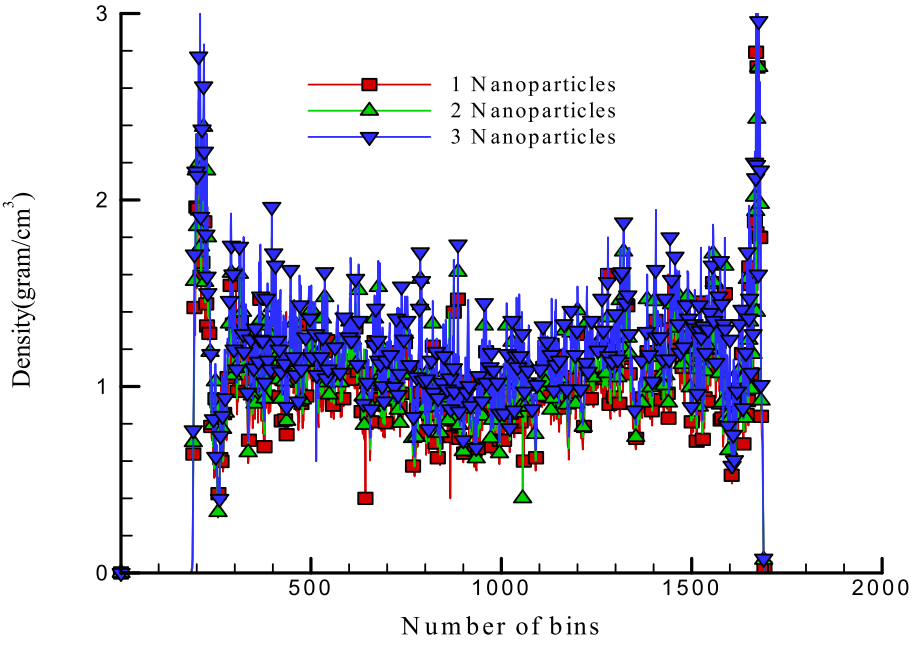


**Fig. 5.** Density profile of $H_2O$/CuO NF over the number of NPs.

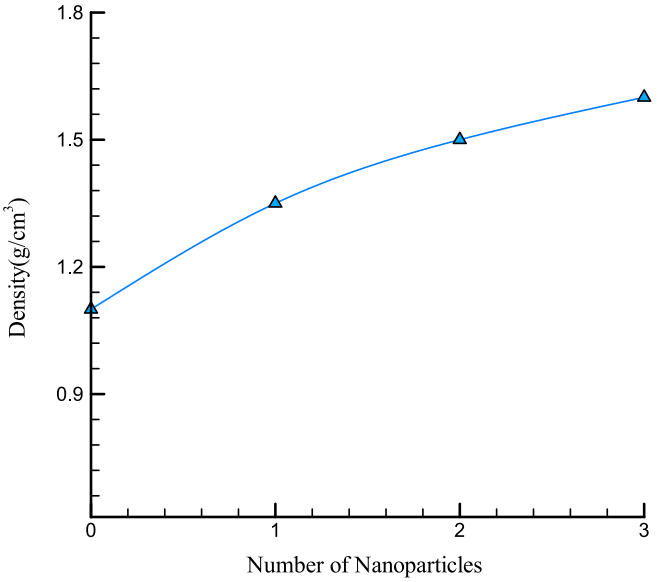


**Fig. 6.** Density profile of $H_2O$/CuO NF particles versus CuO NPs number after t = 1 ns.

**Table 4**
The Highest value of density, temperature, and velocity in $H_2O$/CuO NF by the different numbers of CuO NPs.

| Number of NPs | Maximum Density (atom/Å $^3$) | Maximum Temperature (K) | Maximum Velocity (Å/fs) |
|---|---|---|---|
| 1 | 1.35 | 274 | 0.0073 |
| 2 | 1.50 | 285 | 0.0110 |
| 3 | 1.60 | 303 | 0.0122 |

$k_\theta$ shows the angular constant of an oscillator, and $\theta_0$ defines the equilibrium of the oscillator's angle. We used the harmonic formalism with atomic constants reported in SPC and UFF force fields for the dihedral interaction description. Eq. (4) describes the potential of EAM [12,59].

$$U_i = F_\alpha\left(\sum_{i\neq j}\rho_\beta(r_{ij})\right) + \frac{1}{2}\sum_{i\neq j}\phi_\beta(r_{ij}) \tag{4}$$

In above equation,$\phi_\beta(r_{ij})$ represents the a repulsive force caused by atomic charge density, and $F_\alpha$ function shows the potential bounded. Finally, the total energy of the atomic structure was calculated by Hamilton with this formula [44],

$$\mathrm{H}(r,P) = \frac{1}{2m}\sum_i P_i^2 + V(r_1 + r_2 + \ldots + r_n) = E \tag{5}$$

where V is a potential energy function, E is total energy, P is momentum.

Table 2 shows the all simulation parameters of this study.

## 3. Results and discussion

### 3.1. Equilibration procedure

Firstly, $H_2O$/CuO NF and Pt microchannel system equilibrated at $T_0$ = 300 K for t = 1 ns. This atomic system in different numbers of NPs is shown in Figs. 1 and 2. Fig. 1 shows the direction of force and the presence of NPs in the microchannel after 1 ns. According to the shape and presence of NPs, the results show that the NPs were stable after 1 ns in the microchannel, which indicated the correct selection of potentials (EAM and SPC/UFF) in the previous stage [34,36].

Fig. 3 (a, b) show the temperature, and total energy changes over MD time and the number of CuO NPs. According to Fig. 3, we can say the energy equilibrated after t = 1 ns. Moreover, total energy converged to −533791 eV, −542811 eV, and −553088 eV in the presence of 1, 2, and 3 NPs (see Fig. 3 and Table 3). In examining the temperature, according to equation (6), the temperature depended on the kinetic energy, which also depended on the velocity of atoms [60].

$$Average\ \ Kinetic\ \ Energy = \frac{1}{2}mv^2 = \frac{3}{2}K_B T \tag{6}$$

Based on the results obtained, for 1 and 2 NPs, the level of kinetic energy did not increase significantly because the two atoms were far apart in the channel. However, when there were three atoms in the nanochannel, atomic oscillations increased, and more attractive and repulsive forces

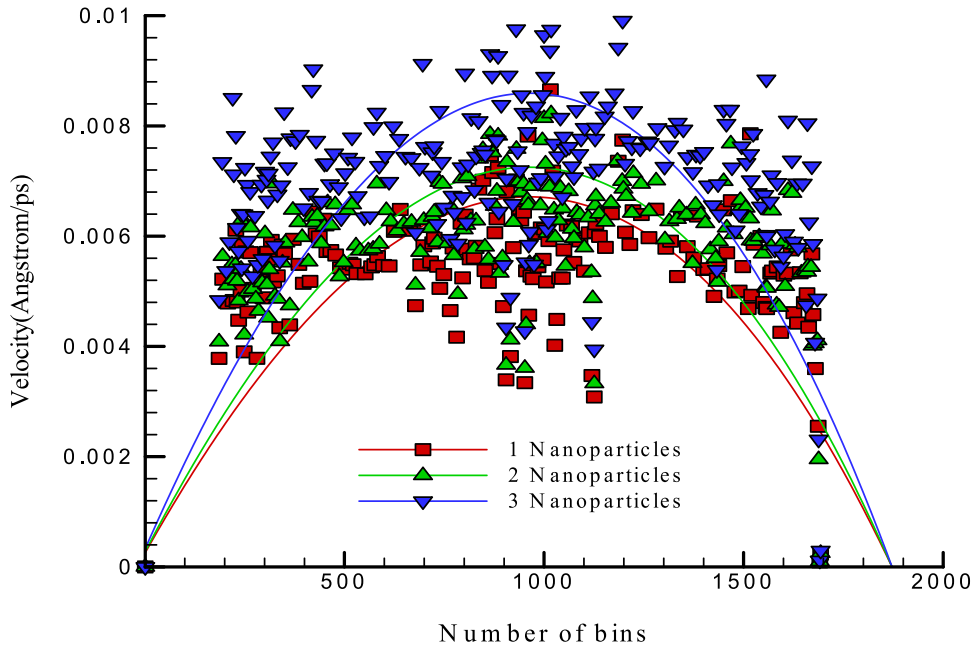


**Fig. 7.** The velocity profile of $H_2O$/CuO NF particles due to CuO NPs number.

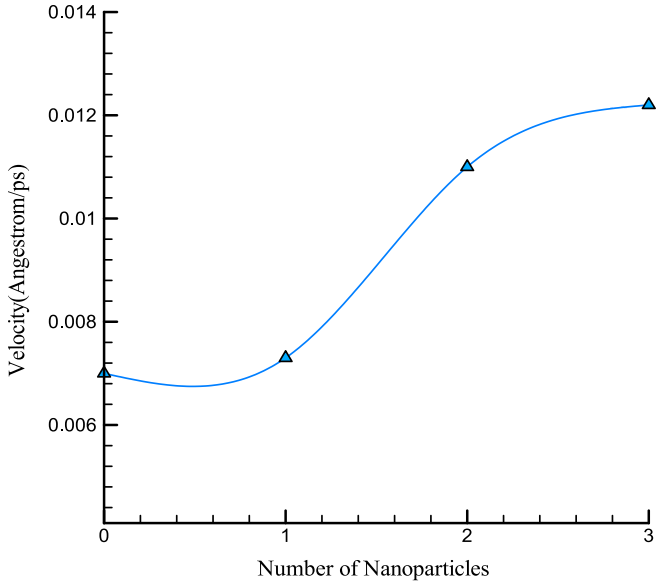


**Fig. 8.** The velocity profile of $H_2O$/CuO NF at the different number of CuO NPs number after t = 1 ns.

were established among three atoms. Consequently, the level of kinetic energy increased, and this led to a significant temperature increase compared to the previous two states.

Since the total energy was equal to the sum of the kinetic energy and the potential energy, and the potential energy in the state of three atoms was less than that of two atoms, as a result, the total energy of three NPs will be less than that of two particles and one particle [61,62].

This atomic behavior showed decreasing atoms' oscillation adequacy by simulation time passing and by adding CuO NPs to $H_2O$ molecules. By occurring this phenomenon, atomic stability was recognized.

In the final step of this part, the radial distribution function of the simulated fluid sample was investigated. RDF changed as the phase of the simulated samples varied, as can be observed in Fig. 4a. It is possible to infer from Fig. 4(a) that structures with a solid phase had many repeated peaks in the RDF. The RDF for atomic structures with a gas phase exhibited a peak at small distances and no peak at longer distances, and the value of g(r) converged to a constant [63]. The RDF of a liquid was intermediate between the solid and gas phases, with a small number of peaks at short distances superimposed on a steady decay to a constant value at longer distances [64]. RDF was calculated via the following equation [65]:

$$g_i(r)dr = \frac{1}{N}\sum_{i=1}^{N} g_i(r)dr \tag{7}$$

RDF of atomic samples showed how the atoms were arranged in nanostructures and offered exact information on where two distinct atoms were in respect to one another in the simulation box. The radial distribution function indicated how the atoms in a structure were arranged relative to each other [66,67]. In the analysis of the result obtained in this part, the presence of a distinct peak, as well as several repeated peaks indicated the liquid phase in the simulated BF sample. Therefore, it is expected that using an external force on the simulated fluid, it is possible to flow and transfer heat inside the aluminum nanochannel.

### 3.2. Atomic behavior of simulated atomic structures

Fig. 5 shows the repartition of NPs inside Pt microchannel over the number of NPs in $H_2O$ molecules. MD results in this section indicated NF particles attracted by Pt atoms as microchannel walls. Therefore, the density value of NF particles had the highest ratio in these sections. Furthermore, the density value of $H_2O$/CuO NF particles decreased in the middle bins of the Pt channel. Moreover, we can say that by enhancing CuO NPs from one to three numbers, the highest value of density varied from 1.35 g/cm$^3$ to 1.60 g/cm$^3$, as reported in Fig. 6 and Table 4. From these listed numerous results, we conclude the NPs numbers affected NF particle arrangement, and the density of the final structure increased by NPs numbers.

The velocity of the simulated $H_2O$/CuO NF is another parameter that can describe the atomic behavior of the NF structure. The velocity profile of $H_2O$/CuO NF particles changed as a function of the number of CuO NPs in this computational study. Fig. 7 illustrates the distribution of velocity of NF particles as a function of the number of CuO NPs in the MD box. This numerical analysis concluded that the highest velocity

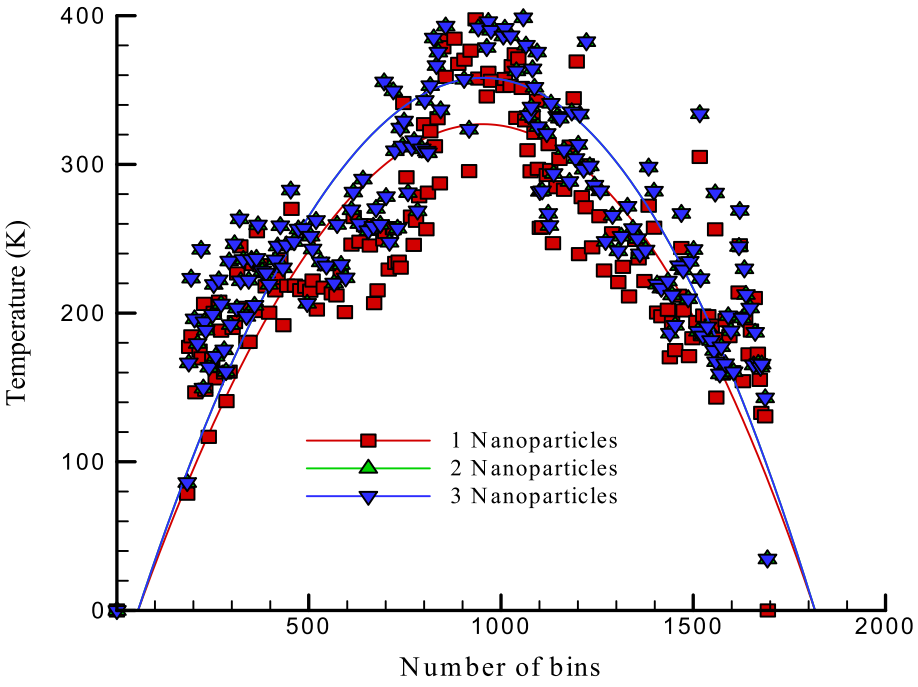


**Fig. 9.** Temperature profile of $H_2O$/CuO NF particles in terms of CuO NPs number.

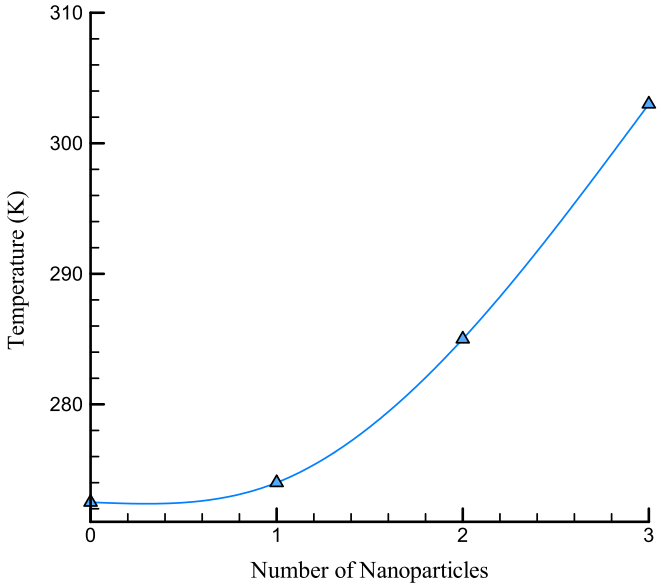


**Fig. 10.** Temperature profile of $H_2O$/CuO NF particles in terms of CuO NPs number after t = 1 ns.

value was located in the middle region of the MD box. In this region, the interaction among $H_2O$/CuO NF particles and Pt atoms, as simulated in the microchannel, converged to a minimum ratio. As a result, $H_2O$/CuO NF particles were freely displaced.

Thus, this atomic parameter became minimum ratios in the initial and final area of box. It indicated the poiseuille flow of simulated NF particles in Pt ideal microchannel. As shown in Fig. 8, by CuO NPs numbers increasing in microchannel, the velocity of $H_2O$/CuO NF improved. The expansion of NPs into the fluid increased the atomic movement in this sample. Therefore, the amount of velocity increased. By increasing movement of atomic structures, the amount of their corresponding oscillations increased, and aggregation in these atomic structures occurred in a shorter period. According to Table 4, the highest velocity value of simulated NF with one NP is 0.0073 Å/ps. By inserting 3 atoms of CuO NPs into the BF, velocity converged to 0.0122 Å/ps. This atomic behavior emerged from external force increasing in simulated NF particles by increasing NP numbers.

The atomic temperature of $H_2O$/CuO NF is shown in Figs. 9 and 10 as a function of NP numbers. Physically, this parameter can show the time progress of simulated NPs. MD simulation results show the temperature attains the maximal amount in the center area of box. This atomic factor attained the least amount in the initial/final MD package. The highest $H_2O$/CuO NF temperature was 274 K, 385 K, and 303 K in the presence of 1, 2, and 3 NPs, respectively (see Table 4). The simulated movement had the same behavior as shown in Fig. 8. This parameter attained the highest value in the center area of MD simulation box which was focalized to the minimum proportion in the vicinity of Pt atoms. From our results from this section of our MD study, we conclude that CuO NPs numbers increased in $H_2O$ BF, and the final NF's atomic movement was appreciable.

### 3.3. *Aggregation process of simulated atomic structures*

Fig. 11 shows atomic exhibition of CuO NPs aggregation process in $H_2O$/CuO NF flow in Pt microchannel at different time. Based on Fig. 11, at the beginning of the simulation, two atoms were far apart from each other. After 0.5 ns, two atoms start to approach each other due to the attractive forces, and the intermolecular distance decreased over the course of 1 ns. After 1 ns, the two atoms stuck together, and according to the energy level diagram, their energy levels reached their lowest value, indicating the aggregation process. NPs' aggregation procedure was another parameter in NFs structures. This process can be affected by NP number changes. According to results of Table 5, aggregation at $T_0$ = 300 K, AT achieved t = 1.15 ns and t = 1.01 ns in the presence of 2 and 3 numbers CuO NPs. This process happened because the atomic oscillation amplitude increased by the number of NPs increasing in the MD simulation box. The atomic movement of different NPs of $H_2O$/CuO NF increased by NPs number increasing, and NPs aggregation phenomenon was recognized faster. CuO NPs aggregation procedure is shown in Fig. 11.

Moreover, the PE of simulated structures increased by increasing the

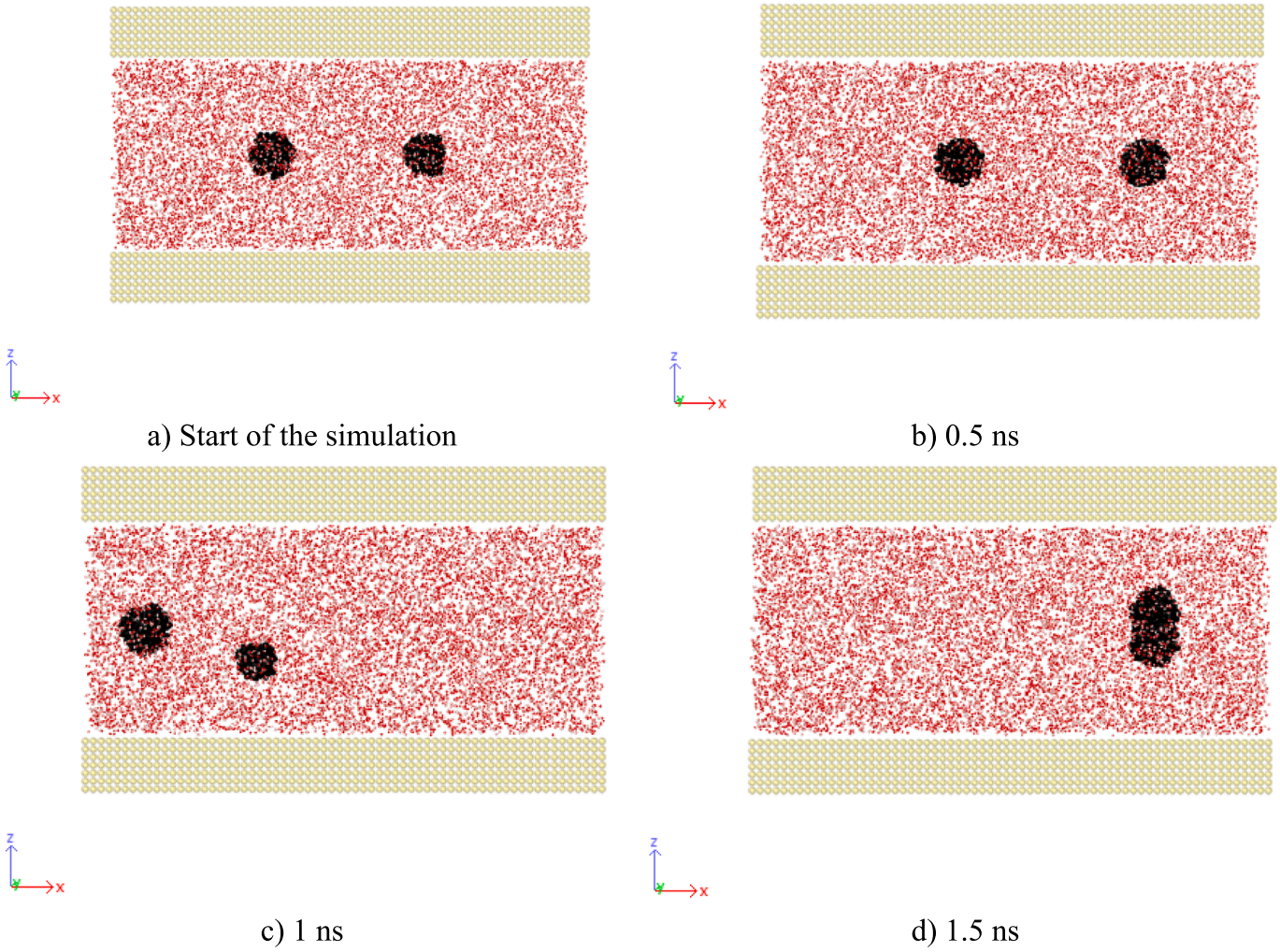


**Fig. 11.** Atomic exhibition of CuO NPs aggregation process in $H_2O$/CuO NF flow in Pt microchannel at different time.

**Table 5**
The changes of AT and PE of $H_2O$-CuO NF in terms of NPs number.

| Number of NPs | AT (ns) | PE (eV) |
|---|---|---|
| 2 | 1.15 | −652411 |
| 3 | 1.01 | −660258 |

number of NPs. From the numerical point of view, the PE in the last point of simulations changed from −652411 to −660258 eV (see Fig. 12).

The main reason for the NP aggregation phenomenon observed in this study was the applied external force, which caused the NPs to move and get closer to each other. When the NPs approached each other closely due to the high intensity of their interaction compared to the BF particles, aggregation occurred. As the NPs stuck to each other, the fluid-NP interface decreased, leading to a reduction in the number of collisions among the NPs and the BF. As the collisions decreased, PE and enthalpy of the system decreased. Therefore, in the time steps related to the aggregation of NPs, the system was momentarily out of equilibrium, and the system's energy level decreased step by step. The system energy was then rebalanced until the next aggregation. This process continued until all the NPs adhered so that the system eventually reached the minimum energy level, and fluctuations in the system increased.

## 4. Conclusion

In summary, the atomic behavior of structure and the effect of the number of CuO NPs on the aggregation process in $H_2O$/CuO NF in a Pt microchannel was performed using the MD simulation. Various physical factors, such as density, temperature, velocity, AT, and PE were calculated. This simulation was done with LAMMPS software. In these estimations, $H_2O$ molecules were defined as a BF in which 1, 2, and 3 numbers of CuO NPs with a spherical shape were appended to the BF. The simulation time was 5 ns. The results of MD calculations were as takes after:

By enhancing CuO NPs from one to three numbers, the highest value of density varied from 1.35 g/cm$^3$ to 1.60 g/cm$^3$. The NPs numbers affected NF particle arrangement, and the density of the final structure increased by NPs numbers.

The highest velocity value was located in the middle region of the MD box. In this region, the interaction among $H_2O$/CuO NF particles and Pt atoms, as simulated in the microchannel, converged to a minimum ratio. By inserting 3 atoms of CuO NPs into the BF, velocity converged to 0.0122 Å/ps.

The highest $H_2O$/CuO NF temperature was 274 K, 385 K, and 303 K in the presence of 1, 2, and 3 NPs, respectively.

A significant decrease in the potential energy diagram indicates the occurrence of the lumping process. This process can be prevented by checking the potential energy.

NPs' aggregation procedure was another parameter in NFs

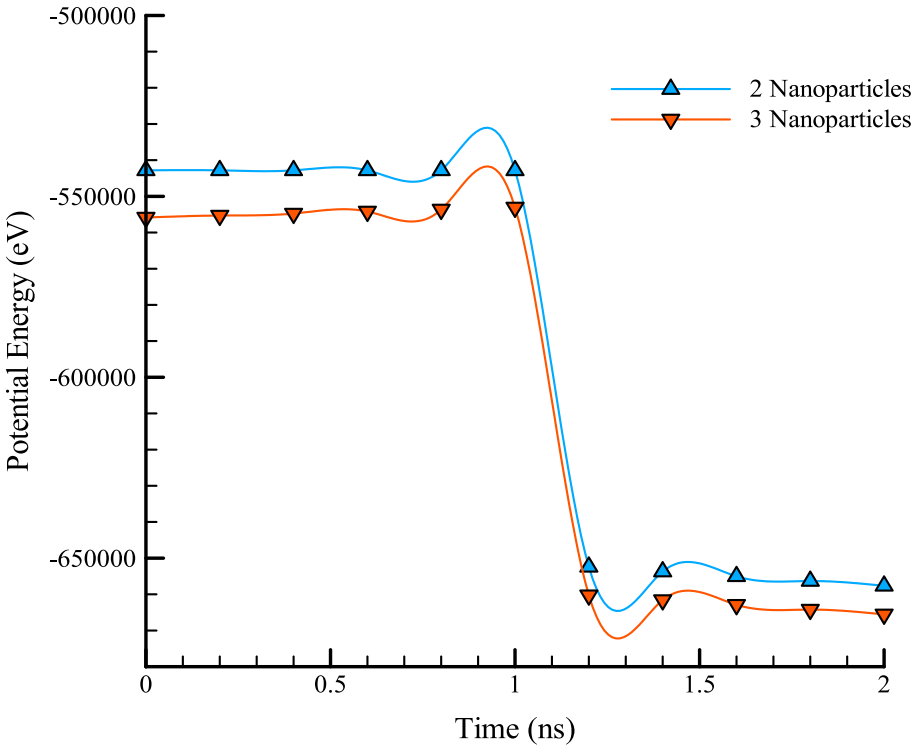


**Fig. 12.** The changes of PE in CuO NPs number inside MD simulation box.

structures. This process can be affected by NP number changes. According to results of Table 5, aggregation at $T_0 = 300$ K, AT achieved t = 1.15 ns and t = 1.01 ns in the presence of 2 and 3 numbers CuO NPs.

## 5. Suggestions

It was suggested that the effect of an external field on the amount of aggregation be studied. It is possible to consider the effect of aggregation of NPs on the TC and viscosity of NFs. It investigated the effect of parameters like the size of NPs, particle volume fraction, and the intensity of the fluid-NP interface at the aggregation rate.

## Declaration of Competing Interest

The authors declare that they have no known competing financial interests or personal relationships that could have appeared to influence the work reported in this paper.

## Acknowledgements

Gansu Provincial Natural Science Foundation Project, 22jr11ra235, Computer simulation analysis and research on Time Wheel Calendar of ancient Tibetan calendars.

Central University Project of Northwest Minzu University, 31920230064, Computer Simulation Analysis and Research on Time Wheel Calendar.

## References

[1] Z. Alrowaili, M. Ezzeldien, N.M. Shaaalan, E. Hussein, M. Sharafeldin, Investigation of the effect of hybrid CuO-Cu/water nanofluid on the solar thermal energy storage system, J. Storage Mater. 50 (2022), 104675.

[2] N.S. Mane, V. Hemadri, Experimental investigation of stability, properties and thermo-rheological behaviour of water-based hybrid CuO and Fe3O4 nanofluids, Int. J. Thermophys. 43 (1) (2022) 1–22.

[3] H. Ajdari, A. Ameri, Performance assessment of an inclined stepped solar still integrated with PCM and CuO/GO nanocomposite as a nanofluid, J. Build. Eng. (2022), 104090.

[4] C. Nwaokocha, M. Momin, S. Giwa, M. Sharifpur, S. Murshed, J. Meyer, Experimental investigation of thermo-convection behaviour of aqueous binary nanofluids of MgO-ZnO in a square cavity, Therm. Sci. Eng. Progr. 28 (2022), 101057.

[5] H. Zare Aliabadi, M. Saei Moghaddam, Experimental investigation of the effect of zinc oxide nanoparticles and process parameters on thermal performance of flat plate solar collector, Nashrieh Shimi va Mohandesi Shimi Iran (2020).

[6] Y. Shang, R.B. Dehkordi, S. Chupradit, D. Toghraie, A. Sevbitov, M. Hekmatifar, W. Suksatan, R. Sabetvand, The computational study of microchannel thickness effects on H2O/CuO nanofluid flow with molecular dynamics simulations, J. Mol. Liq. 345 (2022), 118240.

[7] Y.-L. Sun, D. Toghraie, O.A. Akbari, F. Pourfattah, A.A. Alizadeh, N. Ghajari, M. Aghajani, Thermal performance and entropy generation for nanofluid jet injection on a ribbed microchannel with oscillating heat flux: Investigation of the first and second laws of thermodynamics, Chin. J. Chem. Eng. 42 (2022) 450–464.

[8] R. Manimaran, K. Palaniradja, N. Alagumurthi, S. Sendhilnathan, J. Hussain, Preparation and characterization of copper oxide nanofluid for heat transfer applications, Appl. Nanosci. 4 (2014) 163–167.

[9] D.P. Barai, B.A. Bhanvase, G. Żyła, Experimental investigation of thermal conductivity of water-based Fe3O4 nanofluid: An effect of ultrasonication time, Nanomaterials 12 (12) (2022) 1961.

[10] H.K. Judran, A.G.T. Al-Hasnawi, F.N. Al Zubaidi, W.A.K. Al-Maliki, F. Alobaid, B. Epple, A high thermal conductivity of MgO-H2O nanofluid prepared by two-step technique, Appl. Sci. 12 (5) (2022) 2655.

[11] M. Ghasemi, M. Niknejadi, D. Toghraie, Direct effect of nanoparticles on the thermal conductivity of CuO-water nanofluid in a phase transition phenomenon using molecular dynamics simulation, J. Therm. Anal. Calorim. 144 (6) (2021) 2483–2495.

[12] A. Mosavi, M. Hekmatifar, A.A. Alizadeh, D. Toghraie, R. Sabetvand, A. Karimipour, The molecular dynamics simulation of thermal manner of Ar/Cu nanofluid flow: the effects of spherical barriers size, J. Mol. Liq. 319 (2020), 114183.

[13] D. Toghraie, M. Hekmatifar, Y. Salehipour, M. Afrand, Molecular dynamics simulation of Couette and Poiseuille Water-Copper nanofluid flows in rough and smooth nanochannels with different roughness configurations, Chem. Phys. 527 (2019), 110505.

[14] S. Jiang, S.A. Jasim, S. Danshina, M.Z. Mahmoud, W. Suksatan, D. Toghraie, M. Hekmatifar, R. Sabetvand, Molecular dynamics simulation the effect of initial pressure on the phase transition performance of coated AlH3 nanoparticles in the presence of an oxygenated medium, J. Mol. Liq. (2022), 119183.

[15] Q. Liu, O. Bykanova, R. Akhmadeev, S. Baghaie, M. Hekmatifar, A. Arefpour, R. Sabetvand, V. Borisov, The numerical study of pressure and temperature effects on mechanical properties of baghdadite-based nanostructure: molecular dynamics simulation, Sci. Rep. 12 (1) (2022) 1–12.

[16] M.S. Zarei, A.T.K. Abad, M. Hekmatifar, D. Toghraie, Heat transfer in a square cavity filled by nanofluid with sinusoidal wavy walls at different wavelengths and amplitudes, Case Stud. Thermal Eng. 34 (2022), 101970.

[17] A. Hassanvand, M. Saei Moghaddam, M. Barzegar Gerdroodbary, Y. Amini, Analytical study of heat and mass transfer in axisymmetric unsteady flow by ADM, J. Comput. Appl. Res. Mech. Eng. (JCARME) 11 (1) (2021) 151–163.
[18] S. Ahadian, H. Mizuseki, Y. Kawazoe, An efficient tool for modeling and predicting fluid flow in nanochannels, J. Chem. Phys. 131 (18) (2009), 184506.
[19] P.G. Jamkhande, N.W. Ghule, A.H. Bamer, M.G. Kalaskar, Metal nanoparticles synthesis: An overview on methods of preparation, advantages and disadvantages, and applications, J. Drug Delivery Sci. Technol. 53 (2019), 101174.
[20] H. Dong, J. Zhao, J. Chen, Y. Wu, B. Li, Recovery of platinum group metals from spent catalysts: a review, Int. J. Miner. Process. 145 (2015) 108–113.
[21] R. Taylor, S. Coulombe, T. Otanicar, P. Phelan, A. Gunawan, W. Lv, G. Rosengarten, R. Prasher, H. Tyagi, Small particles, big impacts: A review of the diverse applications of nanofluids, J. Appl. Phys. 113 (1) (2013) 1.
[22] J. Buongiorno, Convective transport in nanofluids, 2006.
[23] S. K. Das, S. U. Choi, W. Yu, T. Pradeep, *Nanofluids: science and technology*: John Wiley & Sons, 2007.
[24] A. Hassanvand, S.H. Esmaeili-Faraj, M.S. Moghaddam, R. Moradi, Characterization of a new structured packing by computational fluid dynamics, Chem. Eng. Technol. 44 (1) (2021) 156–163.
[25] Y. Shi, A. Abidi, Y. Khetib, L. Zhang, M. Sharifpur, G. Cheraghian, The computational study of nanoparticles shape effects on thermal behavior of H2O-Fe nanofluid: A molecular dynamics approach, J. Mol. Liq. 346 (2022), 117093.
[26] Y. Shi, S.M. Sajadi, M.A. Alazwari, P. Firouzi, N.H. Abu-Hamdeh, F. Ghaemi, D. Baleanu, A. Karimipour, The Molecular dynamics study of atomic Management and thermal behavior of Al-Water Nanofluid: A two phase unsteady simulation, J. Mol. Liq. 340 (2021), 117286.
[27] T.T. Baby, S. Ramaprabhu, Investigation of thermal and electrical conductivity of graphene based nanofluids, J. Appl. Phys. 108 (12) (2010), 124308.
[28] R. Prasher, W. Evans, P. Meakin, J. Fish, P. Phelan, P. Keblinski, Effect of aggregation on thermal conduction in colloidal nanofluids, *Appl. Phys. Lett.,* 89 (14) 2006.
[29] P. Shima, J. Philip, B. Raj, Influence of aggregation on thermal conductivity in stable and unstable nanofluids, *Appl. Phys. Lett.,* 97 (15), 2010.
[30] S. Batista, C. a.; Larson, RG; Kotov, N. a. Nonadditivity of nanoparticle interactions, Science 350 (2015) 1242477.
[31] Y. Shi, S.M. Sajadi, M.A. Alazwari, P. Firouzi, N.H. Abu-Hamdeh, F. Ghaemi, D. Baleanu, A. Karimipour, The molecular dynamics study of atomic management and thermal behavior of al-water nanofluid: a two phase unsteady simulation, J. Mol. Liq. (2021), 117286.
[32] C.-C. Chen, C. Zhu, E.R. White, C.-Y. Chiu, M. Scott, B. Regan, L.D. Marks, Y. Huang, J. Miao, Three-dimensional imaging of dislocations in a nanoparticle at atomic resolution, Nature 496 (7443) (2013) 74–77.
[33] H. Kang, Y. Zhang, M. Yang, L. Li, Molecular dynamics simulation on effect of nanoparticle aggregation on transport properties of a nanofluid, J. Nanotechnol. Eng. Med. 3 (2) (2012), 021001.
[34] R.B. Dehkordi, D. Toghraie, M. Hashemian, F. Aghadavoudi, M. Akbari, Molecular dynamics simulation of ferro-nanofluid flow in a microchannel in the presence of external electric field: Effects of Fe3O4 nanoparticles, Int. Commun. Heat Mass Transfer 116 (2020), 104653.
[35] X.-Y. Shen, M. Hekmatifar, M.Y.A. Shukor, A.A. Alizadeh, Y.-L. Sun, D. Toghraie, R. Sabetvand, Molecular dynamics simulation of water-based Ferro-nanofluid flow in the microchannel and nanochannel: effects of number of layers and material of walls, J. Mol. Liq. (2021), 116924.
[36] R.B. Dehkordi, D. Toghraie, M. Hashemian, F. Aghadavoudi, M. Akbari, The effects of external force and electrical field on the agglomeration of Fe3O4 nanoparticles in electroosmotic flows in microchannels using molecular dynamics simulation, Int. Commun. Heat Mass Transfer 122 (2021), 105182.
[37] P. Mark, L. Nilsson, Structure and dynamics of the TIP3P, SPC, and SPC/E water models at 298 K, Chem. A Eur. J. 105 (43) (2001) 9954–9960.
[38] W.L. Jorgensen, C. Jenson, Temperature dependence of TIP3P, SPC, and TIP4P water from NPT Monte Carlo simulations: seeking temperatures of maximum density, J. Comput. Chem. 19 (10) (1998) 1179–1186.
[39] Y. Song, L.L. Dai, The shear viscosities of common water models by non-equilibrium molecular dynamics simulations, Mol. Simul. 36 (7–8) (2010) 560–567.
[40] Y. Zheng, X. Zhang, M.T. Soleimani Mobareke, M. Hekmatifar, A. Karimipour, R. Sabetvand, Potential energy and atomic stability of H2O/CuO nanoparticles flow and heat transfer in non-ideal microchannel via molecular dynamic approach: the green–Kubo method, J. Therm. Anal. Calorim. 144 (6) (2021) 2515–2523.
[41] Y. Zhai, Y. Li, Z. Xuan, Z. Li, H. Wang, Determination of heat transport mechanism using nanoparticle property and interfacial nanolayer in a nanofluidic system, J. Mol. Liq. 344 (2021), 117787.
[42] E. Torres, I. Carrillo-Berdugo, D. Zorrilla, J. Sánchez-Márquez, J. Navas, CuO-containing oil-based nanofluids for concentrating solar power: an experimental and computational integrated insight, J. Mol. Liq. 325 (2021), 114643.
[43] S. Lee, R. Saidur, M. Sabri, T. Min, Effects of the particle size and temperature on the efficiency of nanofluids using molecular dynamic simulation, Num. Heat Transfer, Part a: Appl. 69 (9) (2016) 996–1013.
[44] L. Verlet, Computer" experiments" on classical fluids. I. Thermodynamical properties of Lennard-Jones molecules, Phys. Rev. 159 (1) (1967) 98.
[45] W. Press, S. Teukolsky, W. Vetterling, B. Flannery, Section 17.4. Second-order conservative equations. Numerical Recipes: the Art of Scientific Computing, 3rd ed., Cambridge University Press, New York, 2007.
[46] E. Hairer, C. Lubich, G. Wanner, Geometric numerical integration illustrated by the Störmer-Verlet method, Acta Numerica 12 (2003) 399–450.
[47] D. Brown, J. Clarke, A comparison of constant energy, constant temperature and constant pressure ensembles in molecular dynamics simulations of atomic liquids, Mol. Phys. 51 (5) (1984) 1243–1252.
[48] S. Toxvaerd, Ensemble simulations with discrete classical dynamics, J. Chem. Phys. 139 (22) (2013), 224106.
[49] M. Ghasemi, A. Shafiei, J. Foroozesh, A systematic and critical review of application of molecular dynamics simulation in low salinity water injection, Adv. Colloid Interface Sci. 300 (2022), 102594.
[50] W.G. Hoover, Canonical dynamics: equilibrium phase-space distributions, Phys. Rev. A 31 (3) (1985) 1695.
[51] J. Thijssen, Computational Physics, Cambridge University Press, 2007.
[52] S. Hilbert, P. Hänggi, J. Dunkel, Thermodynamic laws in isolated systems, Phys. Rev. E 90 (6) (2014), 062116.
[53] D. Ms, SM. 170113158? M1 BASKES, Mater. Sci. Rep 9 (1993) 251.
[54] A.K. Rappé, C.J. Casewit, K. Colwell, W.A. Goddard III, W.M. Skiff, UFF, a full periodic table force field for molecular mechanics and molecular dynamics simulations, J. Am. Chem. Soc. 114 (25) (1992) 10024–10035.
[55] J. E. Lennard-Jones, Cohesion, *Proceedings of the Physical Society (1926-1948),* vol. 43, no. 5, pp. 461, 1931.
[56] R.A. Serway, J.W. Jewett, Physics for Scientists and Engineers (with PhysicsNOW and InfoTrac), Brooks Cole Monterey, CA, 2003.
[57] S. I. Hayek, Mechanical vibration and damping, *digital Encyclopedia of Applied Physics*, 2003.
[58] D.C. Rapaport, The Art of Molecular Dynamics Simulation, Cambridge University Press, 2004.
[59] M.S. Daw, M.I. Baskes, Embedded-atom method: Derivation and application to impurities, surfaces, and other defects in metals, Phys. Rev. B 29 (12) (1984) 6443.
[60] R. Kutteh, R. Jones, Rigid body molecular dynamics with nonholonomic constraints: Molecular thermostat algorithms, Phys. Rev. E 61 (3) (2000) 3186.
[61] J. Ischtwan, M.A. Collins, Molecular potential energy surfaces by interpolation, J. Chem. Phys. 100 (11) (1994) 8080–8088.
[62] S. Sato, Potential energy surface of the system of three atoms, J. Chem. Phys. 23 (12) (1955) 2465–2466.
[63] J.M. Sorenson, G. Hura, R.M. Glaeser, T. Head-Gordon, What can x-ray scattering tell us about the radial distribution functions of water? J. Chem. Phys. 113 (20) (2000) 9149–9161.
[64] J.G. Kirkwood, E.M. Boggs, The radial distribution function in liquids, J. Chem. Phys. 10 (6) (1942) 394–402.
[65] G. Harding, A. Harding, X-ray diffraction imaging for explosives detection, in: Counterterrorist detection techniques of explosives, Elsevier, 2007, pp. 199–235.
[66] Y. Wang, J. Zheng, G.F. Smaisim, D. Toghraie, Molecular dynamics simulation of phase transition procedure of water-based nanofluid flow containing CuO nanoparticles, Alex. Eng. J. 61 (12) (2022) 12453–12461.
[67] A. Loya, G. Ren, Molecular dynamics simulation study of rheological properties of CuO–water nanofluid, J. Mater. Sci. 50 (11) (2015) 4075–4082.